TECHNICAL MEMORANDUM

601

Impact of assimilating AMMA soundings on ECMWF analyses and forecasts

Anna Agustí-Panareda, Anton Beljaars, Carla Cardinali, Iliana Genkova and Chris Thorncroft[1]

Research Department

[1]State University of New York, Albany, New York

submitted to Weather and Forecasting

October 2009

European Centre for Medium-Range Weather Forecasts
Europäisches Zentrum für mittelfristige Wettervorhersage
Centre européen pour les prévisions météorologiques à moyen terme

Series: ECMWF Technical Memoranda

A full list of ECMWF Publications can be found on our web site under:
http://www.ecmwf.int/publications/

Contact: library@ecmwf.int

European Centre for Medium-Range Weather Forecasts
Shinfield Park, Reading, RG2 9AX, England

Abstract

The field experiment of the African Monsoon Multidisciplinary Analysis (AMMA) project during the 2006 wet monsoon season provided an unprecedented number of radiosonde/dropsonde data over the West African region. This paper explores the usage and impact of this invaluable dataset in the European Centre for Medium-range Weather Forecasts analyses and forecasts. These soundings are the only source of data that can provide 3-D information of the thermodynamic and dynamic structure of the lower troposphere over continental West Africa. They are particularly important for the Sahel region located between 12^oN and 20^oN which is characterized by large gradients in temperature and moisture in the lower troposphere. Assimilation experiment comparison between pre-AMMA and AMMA radiosonde network shows that the extra AMMA soundings have a significant impact on the low-level temperature over the Sahel and on the structure of the African easterly jet. However, the impact of the extra AMMA data on the forecast disappears after 24 hours. The soundings reveal large model biases in boundary layer temperature over northern and eastern Sahel, which are consistent with the well-known model biases in cloud, rainfall and radiation. Large analysis increments in temperature lead to increments in divergence and subsidence which act to suppress convection. Thus, the analysis increments appear to have an undesirable feedback on the cloud and temperature model bias. The impact of the AMMA soundings on the African easterly jet is to enhance and extend the jet streak to 15^oE, i.e. towards the eastern part of the Sahel. No observations are assimilated east of 15^oE at the level of the African easterly jet to support the jet enhancement further east. Comparison with independent atmospheric cloud motion vectors indicate that the African easterly jet in the analysis is too weak over this data-scarse region. This could have implications for the development of African easterly waves in the model forecast. Further experimentation by assimilating atmospheric motion vectors – currently not used – could address this problem.

1 Introduction

The West African monsoon provides most of the annual precipitation over drought-prone Sahel. However, Numerical Weather Prediction (NWP) precipitation forecast is generally poor during the wet West African monsoon season from June to September, partly because of the lack of data available. Before the African Monsoon Multidisciplinary Analysis (AMMA) field experiment in 2006, the radiosonde network was quite sparse and only few data were received via the Global Telecommunication System (GTS). Therefore, few radiosonde observations were assimilated in NWP analyses. The AMMA project put a large effort on restoring and enhancing the radiosonde network (Parker *et al.*, 2008), which is the only data source that gives comprehensive 3-D thermodynamic and dynamic information of the atmosphere over continental West Africa.

The aim of this paper is to assess the impact of the enhanced AMMA radiosonde network on the European Centre for Medium range Weather Forecasts (ECMWF) analysis and forecast during August 2006, i.e. within the peak of the monsoon season. In order to do this, Observation System Experiments (OSE) were performed by comparing two scenarios: the AMMA scenario with the enhanced radiosonde network versus the pre-AMMA scenario with a degraded radiosonde network comprising only those stations that reliably distributed the data through GTS in 2005.

During the AMMA field experiment the radiosonde humidity data were found to have large biases creating dry pockets in the analysis and degrading the precipitation field in the forecast. Agustí-Panareda *et al.* (2009b) developed a new bias correction scheme for the AMMA radiosondes which leads to an improved precipitation forecast in the ECMWF Integrated Forecasting System (IFS) model. A validation of the corrected AMMA radiosondes shows good agreement with independent ground based Global Positioning System (GPS) total column water vapour (TCWV) at several AMMA sites. Faccani *et al.* (2009) tested the impact of this bias correction scheme on the AMMA soundings in the French assimilation system ARPEGE (Gauthier and Thépaut, 2001; Janisková *et al.*, 1999) during the period between 15 July and 15 September 2006. They also found a positive impact on the precipitation forecast, as well as the conventional forecast scores in the medium range.

The use of the radiosonde humidity bias correction is therefore crucial when assessing the benefit of the AMMA observations on the NWP analysis and forecast.

The structure of the paper is the following. Section 2 describes the pre-AMMA and AMMA radiosonde network. A summary of the data assimilation system used for the experiments is also provided. Sections 3 and 4 show the data impact results and comparisons with independent observations. A discussion on the results is presented in section 5. The main conclusions and suggestions for future work are given in section 6.

2 The AMMA and pre-AMMA observation system experiments

In order to assess the impact of the enhanced radiosonde network during the AMMA Special Observing Period (SOP) two analysis experiments were performed. The first experiment uses all sounding data from the AMMA database (*http://amma-international.org/data/*), as well as all the GTS data received during August 2006 (see table 1) and it is referred to as AMMA. Many stations have high resolution datasets with approximately 3000 levels in the vertical. Before assimilating the high resolution observations it was necessary to apply some thinning. This was done by taking a maximum of 4 vertical measurements per model level. The second experiment is the control experiment which uses only data received via GTS from stations that were reliably reporting to the GTS in 2005, i.e. before the AMMA SOP (see table 2). Thus, it is referred to as pre-AMMA. The total number of soundings available for the two experiments is shown in tables 1 and 2. The stations names and the daily frequencies are shown in Figure 1.

Both experiments are based on the ECMWF IFS model cycle CY32R3. This cycle was operational from 6 November 2007 to 3 June 2008. It includes improved physics with a new formulation of convective entrainment and adjustment, vertical diffusion reduction in the free atmosphere, new soil hydrology and new operational radiosonde temperature and humidity bias correction. Bechtold *et al.* (2008) showed that the changes in the model physical parameterisations lead to an improved precipitation forecast in the short-range over the tropics and in particular over West Africa, where the ITCZ shifts northward by approximately 1 degree (Agustí-Panareda and Beljaars, 2008).

The AMMA radiosonde humidity bias correction of Agustí-Panareda *et al.* (2009b) is also used in both experiments. Almost half of the AMMA radiosondes in 2006 were Vaisala RS80-A which are known to have large dry biases in relative humidity (RH) (Wang *et al.*, 2002). The other main types of radiosondes were MODEM and Vaisala RS92. The RH biases were estimated as a funcion of sonde type, solar elevation, pressure level and observed RH using the Cumulative Distribution Function (CDF) matching technique and Vaisala RS92 at nighttime as reference. The bias correction ranges from 10% to 28 % at low-levels within the boundary layer and 8% to 20 % from 800 to 300 hPa. The validation of the bias correction was done by comparing the corrected radiosonde data with independent ground-based GPS TCWV at 6 sites in the Sahel. The comparison shows that the mean difference between the two datasets ranges between -1 and 1.5 Kg m^{-2}, which is close to the uncertainty of the GPS TCWV data (+/- 1 Kg m^{-2}). Clearly, the use of corrected humidity profiles in the analysis also reduces the TCWV bias with respect to GPS at all sites. The impact on the analyzed TCWV and short-range precipitation forecast is significant. TCWV increases between 2 to 6 kg m^{-2} around the corrected radisonde stations and there is an increase of approximately 2mm day^{-1} in the 1-day precipitation forecast within the latitude band from 8^{o}N to 15 ^{o}N.

The IFS data assimilation system is 4D-Var (Rabier *et al.*, 2000) with a full representation of the linearized physical processes (Janisková *et al.*, 2002; Tompkins and Janisková, 2004; Lopez and Moreau, 2005). The 4D-Var assimilation system provides the estimate of the atmospheric state by combining meteorological observations and a prior model information or background. The solution is a weighted mean of the two datasets (observations and model) and the weights are given by the so-called background error covariance matrix (B-

matrix) and by an estimate of observation error variances (R-matrix). The observations are assimilated within a 12 hour window at the correct time. The background error covariance matrix plays a key role in spreading the information on different pressure levels and away from the observating stations. Furthermore, balance among the model parameters is imposed mainly in the extratropics (Derber and Bouttier, 1999).

Figure 2 displays the distribution of the conventional observations assimilated in August 2006 only below 500 hPa, i.e. the layer which comprises the monsoon flow and the African easterly jet. In this layer, aircraft provide information of wind and temperature in the ascending and descending phase close to the airports. Surface pressure and daytime 2m humidity observations are assimilated from SYNOP over land, ships and buoys. Over the ocean, 10m wind and 2m nighttime humidity are also assimilated from buoys. Observed temperature, wind and humidity profiles from radiosondes and dropsondes are also provided to 4DVar, and wind profiles from sonde pilot balloons are available as well. However, a significant number of the pilot balloon winds are not used because of their inconsistent quality.

Meteosat atmospheric motion vectors (AMVs) from cloud and water vapour feature tracking processed by EUMETSAT (European Organisation for the Exploitation of Meteorological Satellites) are assimilated over the AMMA region with strong restrictions in the lower and mid troposphere. This is due to some known issues with AMV height assignments (see for example Velden *et al.*, 2005; Velden and Bedka, 2009) and the resulting large discrepancy (departure) with the model value at the observation location which can result in a negative impact on the forecast (von Bremen, 2005). Because of that, only high-level AMVs (above 400 hPa) are assimilated in the AMMA domain over land. AMVs from visible channels are used below 400 hPa only over the ocean. Despite these restrictions, monthly statistics for the tropics from EUMETSAT show that AMV and radiosonde profiles are in good agreement for the U and V wind components (see http://cimss.ssec.wisc.edu/iwwg/iwwg_monitoring_amv.html). Thus, it is believed that over the AMMA region, the large discrepancy between model and AMVs are mainly due to model biases.

Scatterometer data and brightness temperatures from satellites were also assimilated over the ocean, providing information of surface wind, temperature and specific humidity. Unfortunately due to the difficulty in the specification of emissivity over land, satellite radiances are not assimilated in the lower troposphere. In summary, the main source of information of the 3-dimensional atmospheric state over the African continent is provided by radiosonde observations.

3 Impact of the AMMA radiosonde network on the analysis

In this section the impact on the analysis of the radiosonde observations from the AMMA campaign is shown. The impact of these data is assessed for temperature, winds and humidity, as well as for cloud coverage. The analysis increments are examined first, followed by a comparison of the mean analysis fields. Finally, independent observations are used to evaluate the results.

3.1 Analysis increments

Temperature, wind and humidity analysis increments (differences between the analysis and 12-hour forecast or background) for the AMMA and pre-AMMA experiments are consistent. Namely, the analysis increments in AMMA reinforce the mean increment pattern already present in pre-AMMA. Moreover, the analysis increments at 00 UTC are mostly in agreement with those at 12 UTC for all parameters. For this reason, the mean increments are computed together for 00UTC and 12 UTC. The largest analysis increments are in the boundary layer and in the mid-troposphere. Thus, pressure levels at 925 hPa and 700 hPa are chosen as the representative

standard levels.

Figure 3a shows the mean analysis increments for temperature and wind at 925 hPa for AMMA. The largest temperature increments are negative and located in the Sahel (12^oN–22^oN) around the observing radiosonde stations. This indicates a temperature reduction in the analysis over Sahel. The temperature reduction is largest at 12 UTC, and less pronounced at 00 UTC (not shown). Over the coast (5^oN–7^oN), Soudanian region (7^ON–12^oN) and in the Sahara (22^oN–35^oN) regions there are mainly positive temperature analysis increments. This brings an increase in temperature in the analysis, notably at nighttime. Overall, the wind increments are against the prevalent south-westerly monsoon flow (Fig. 3b) , particularly in the Sahel. This is consistent with a reduction in the north-south temperature gradient seen here and the associated reduction in north-south pressure gradient (not shown).

It is also worth noting that around several stations in the Sahel (e.g. Tombouctou, N'Djamena and Agadez) the horizontal wind vector increments are divergent and the vertical wind is subsiding (solid black contours in Fig. 3a), providing an unrealistic circulation.

The analysis increments for temperature (Fig. 3a) are similar throughout the pressure layer between surface and 850 hPa over the Sahel and from the surface to 925 hPa in the regions near the coast, Soudanian region and over Sahara. At 700 hPa the mean temperature analysis increments are very small in magnitude (not shown).

Figure 4 shows the mean analysis increments for the zonal wind at 700 hPa. A dipole of negative and positive increments north and south of 15^oN implies that the African easterly jet (AEJ) is displaced northwards in the analysis. The jet is also strengthened by around 1.5 m s^{-1} at the entrance region around 15^oN and 15^oE, surrounding the radiosonde station of N'Djamena. This increase of the wind speed around 15^oN is enhanced during the daytime. Another region where there is an increase in the speed of the AEJ is around Tombouctou (16.43^oN, 3.00^oW). Note that data from both N'Djamena and Tomboctou are not available in pre-AMMA.

The analysis increments for the meridional winds (not shown) reduce the northerly wind in the eastern Sahel (east of 15^oE) and increase the northerly wind west of 5^oE mainly during the daytime. This results in a more zonal jet. At nighttime, the analysis increments at the latitude of the jet are small in magnitude and in area coverage.

Figure 5a shows the vertical profile of mean observation departures for specific humidity in the whole West African region (5^oN to 30^oN and 20^oW to 20^oE). Below 850 hPa, the model background is drier than the observations. The dry bias is of the same order of magnitude as the standard deviation of the departures (not shown). The analysis increments – depicted by the difference between the dash and solid lines in Fig. 5 – are very small or negligible at 925 hPa (see also Fig. 6a). As a result, the specific humidity analysis at low-levels over the whole region is also drier than the bias-corrected radiosonde measurements. Although the overall specific humidity analysis increments are very small near the surface, the relative humidity increments (not shown) are large, reflecting the large temperature increments described above. It is also worth noting that the bias-corrected radiosonde humidity was found to have a moist bias in TCWV with respect to ground-based GPS observations (Agustí-Panareda *et al.*, 2009b).

Over the Sahel, the model background has a moist bias close to the boundary layer top – around 850 hPa – depicted by a small kink in the observation departures in Fig. 5b. The analysis increments are able to reduce effectively this moist bias by removing moisture from the analysis (Fig. 6b). In the mid-troposphere (between 700 to 400 hPa), the dry bias in the model background is reduced in the analysis for the whole West African region (Fig. 5b).

3.2 Mean analysis

The mean low-level temperature for the AMMA analysis is shown Fig. 7a. The strong positive thermal gradient is responsible for the presence of the AEJ which dominates the West African region during the summer months (Thorncroft *et al.*, 2003). The mean 925 hPa temperature in AMMA is around 2K cooler than in pre-AMMA in the vicinity of Agadez (7.98^{o}E, 16.97^{o}N) and extending over the region 5^{o}W–15^{o}E and 10^{o}N–25^{o}N (Fig. 7b). The fact that the main reduction in temperature occurs between 15^{o}N and 22^{o}N means that the gradient between southern (12^{o}N to 15^{o}N) and northern (15^{o}N and 22^{o}N) Sahel becomes weaker. Conversely, the temperature gradient between northern Sahel and Sahara becomes stronger, suggesting a northward shift of the gradient.

The mean sea level pressure (MSLP) is characterized by a centre or belt of minimum pressure associated with the heat low around the latitude band centred around 22^{o}N (not shown). The mean MSLP difference between AMMA and pre-AMMA shows an increase mainly in the region around Agadez (not shown), which is consistent with the decrease in the mean temperature described above.

The monsoon flow at low-levels plays a key role in the moisture advection over Sahel. It expands throughout the layer from the surface to 850 hPa over central (10^{o}W–10^{o}E) and eastern Sahel, but only up to 925 hPa in western Sahel (west of 10^{O}W). The 925 hPa wind field is used here to depict the low-level monsoon flow. The overall impact of the AMMA data on the low-level monsoon flow is shown in Figure 7c by comparing the AMMA mean analysis with pre-AMMA. The south-westerly flow at 925 hPa is stronger near the coast in the region 5^{o}W–10^{o}E and 0^o–10^{o}N. Between Tamanrasset and Agadez (in the region from 17^{o}N–21^{o}N, 0^o–10^{o}E) the south-westerly monsoon flow is also much stronger. However, the largest impact is on southern flank of the heat low. This is the region where the MSLP gradient (not shown) is strongest and the 925 hPa wind within the south-westerly monsoon flow is fastest (4 to 8 m s^{-1}, see Fig. 3b). The monsoon flow is between 1 and 3 m s^{-1} slower in AMMA, particularly west of N'Djamena and Tombouctou (Fig. 7c). The reason why the difference is mainly upstream of these two stations can be explained by the divergent analysis increments located over Tombouctou, Agadez and N'Djamena in the AMMA experiment (see Fig. 3a). The difference in mean vertical velocity also reveals an increase in subsidence over these three stations (not shown), with up to 0.1 Pa/s increase in the downward mean vertical velocity over N'Djamena.

In the mid-troposphere, the AEJ dominates the flow from 750 to 500 hPa. It is one of the most characteristic components of the West african monsoon. It is particularly well-known for its key role in the North Atlantic tropical cyclogenesis through the development of African easterly waves (e.g. Berry and Thorncroft, 2005). The mean zonal wind analysis difference at 700 hPa between the two experiments shows that there is a large impact from the extra AMMA observations on the structure of the AEJ (Fig. 8). The jet streak associated with the AEJ extends east of 10^{o}E in the AMMA experiment whereas in pre-AMMA the easterly winds in the jet entrance region (5^{o}E–15^{o}E) are much weaker by approximately 2 m s^{-1}.

There is a small impact of the enhanced AMMA radiosonde network on the African tropical easterly jet at 150 hPa and 200 hPa over the Gulf of Guinea (not shown). In AMMA the tropical easterly jet is stronger by approximately 1 m s^{-1}. However, observation departures (not shown) indicate that the strength of the tropical easterly jet over Western Africa is overestimated at the core by $\sim$ 1m s^{-1}. This is probably a consequence of the enhanced convection over the Soudanian and southern Sahel regions, associated with an overestimation of the low-level humidity from the corrected AMMA radiosonde observations (Agustí-Panareda *et al.*, 2009a).

Humidity is one of the key parameters for forecasting precipitation. The impact of the AMMA observations on the analyzed TCWV will help to interpret the radiosonde impact on the precipitation forecast presented in section 4. Comparison of mean TCWV analysis for both experiments (Fig. 9) shows an increase between 1 and 3 kg m^{-2} in the region 5–11 ^{o}N and 1^{o}W–7^{o}E (i.e. in the vicinity of Parakou) as well as in the regions between Agadez, Tamanrasset (i.e. 3^{o}E–13^{o}E, 16^{o}N–25^{o}N) and Tambacounda (13.77^{o}N, 13.68^{o}W). On the other hand,

the areas around Tombouctou and N'Djamena show a significant decrease in TCWV of around 2 kg m^{-2}. The regions with decreased TCWV correspond to regions with enhanced negative humidity analysis increments in the vicinity of the boundary layer top and downward vertical velocity increments within the boundary layer in the AMMA versus pre-AMMA experiments (described in the previous section). Similarly, regions with increased TCWV are associated with larger positive humidity analysis increments in the AMMA experiment.

3.3 Evaluation using independent observations

The impact of the observations are evaluated by comparing the two experiments with independent observations. Since Meteosat-8 AMVs are not assimilated in the analysis below 400 hPa over land (see section 2), they are used as independent evaluation of the analyzed structure of the AEJ. The presence of cold cloud tops is assessed using Meteosat-8 infrared images which are also not assimilated.

The AMV data was gridded at 2 degrees resolution from 750 hPa to 500 hPa to cover the vertical layer of the AEJ. The mean zonal wind from the AMVs and the two analysis experiments during August 2006 for the same layer is plotted in Figure 10. In general, there are large differences in the structure of the AEJ between AMVs and the experiments. In the jet exit (around 15^oW) the easterly wind speeds are stronger in both AMMA and pre-AMMA compared to AMVs. It is worth noting that most of the radiosonde observations used in the analysis experiments are on the gradient of the zonal wind, not on the core itself. Between 10^oE and 17^oE AMMA has a much stronger jet than pre-AMMA, which does not contain radiosonde observations. This indicates that the model tends to produce a weaker jet than observed. The AMVs extend the jet core further with wind speeds faster than 8 m s^{-1} up to the Red sea (around 40^oE). It is also clear that the location and spread of the jet from the AMVs in Fig. 10a is influenced by the orography (Fig. 10a) as well as the surface temperature gradient (Fig. 7a). In fact, the jet slows down and is displaced southwards by the Darfur mountain range which peaks at 3088 m (equivalent to approximately 720 hPa). This curvature in the jet is not present in the analysis experiments (Fig. 10b,c) because the height of the model orography is only 1000 m over Darfur. Another clear difference can be found in the representation of the southern hemispheric AEJ (AEJ-S). Although the AEJ-S is weaker than its nothern counterpart, Mari *et al.* (2008) found that it played an important role in the inter-hemispheric tranport of biomass burning plumes during the 2006 wet season. AMVs display a much stronger AEJ-S with maximum wind speed of 9 m s^{-1} around the equator, whereas the analyses show a weaker jet (approximately 5 m s^{-1}) located further south, at around 5^oS.

Despite the differences between AMVs and AMMA, a bulk comparison of AMVs with individual radiosonde stations indicates that in the vicinity of the jet core the mean difference is less than 1.5 m s^{-1} (see table 3). The AMV's median and standard deviation are within 2 m s^{-1} of the radiosonde data. Note that the individual collocation approach was not used because it would reduce significantly the data volume for the comparison. Moreover, the bulk comparison shows results very similar to the statistics derived during EUMETSAT operational Meteosat-9 AMV quality monitoring (see section 2).

The TCWV from the AMMA experiment in August 2006 was assessed with independent GPS ground-based data by Agustí-Panareda *et al.* (2009b). TCWV time series from GPS and the AMMA analysis show correlations between 0.7 and 0.9. Results comparing TCWV at six GPS stations indicate that the AMMA analysis is too dry in Tombouctou and too moist in Dakar and Tamale (see Fig. 13 from Agustí-Panareda *et al.* (2009b)), suggesting that the analysis dry bias at low-levels found in Fig. 5 is not widespread over the whole AMMA region.

Figure 11 shows the simulated infra-red brightness temperatures (IR Tb) from AMMA, pre-AMMA and those from Meteosat-8. Cold cloud tops less than 285 K are used to detect deep convection. Within the latitude band 10^oN–15^oN, it is clear that both analysis experiments produce less cold cloud tops than observed. However,

west of 10^{o}E, AMMA shows a large improvement compared to pre-AMMA, with colder mean brightness temperatures. Whilst east of 10^{o}E and particularly around N'Djamena (15^{o}E), the brightness temperatures in AMMA are warmer than in the pre-AMMA experiment. This indicates an undesirable reduction of convective clouds in areas where there was already a deficit compared to observations. Similarly, in the region north of 15^{o}N the mean analyses for both experiments lack deep convective clouds whereas the observations show some at 00 UTC. In summary, AMMA analysis of deep convective cloud is better than pre-AMMA in the denser radiosonde region (20^{o}W - 10^{o}E and 5^{o}N - 15^{o}N)

4 Impact of the AMMA radiosonde network on the forecast

Forecast skill from the AMMA and pre-AMMA experiments is compared in this section. Figure 12 shows the root mean square error ($RMSE = \sqrt{\overline{(FC-OB)^2}}$) of temperature, RH and wind for different forecast (FC) ranges (up to 48 hours) and different pressure levels (925 and 700 hPa) verified against radiosonde observations (OB) for AMMA and pre-AMMA. The evolution of the RMSE is remarkably similar for all parameters. There is a positive impact of the extra AMMA observations in the first 12 to 24 hours, becoming neutral afterwards. The impact is significant with 80% confidence interval up to 12 hours. For some fields, e.g. RH at 925 hPa and zonal wind at 925 hPa, the impact is lost before 12 hours. The reason for this short-lived impact lies in the systematic error associated with the model physics, the processes of which can act on time scales of the order of half a day. This is discussed further in section 5.

One of the most important parameters to forecast during the West African monsoon season is the precipitation. Overall there is an improvement in the mean 1-day precipitation forecast over central Sahel, with a precipitation increase of around 2 mm day^{-1} with respect to pre-AMMA. The overestimation of precipitation in the region of Parakou (9.35^{o}N, 2.62^{o}E) is induced by an overestimation of the observed RH which can be traced back to ground-check problems in the soundings at that station (Nuret, personal communication). In contrast, east of 10^{o}E, the reduced precipitation amount (Fig. 13) collocated with increased subsidence makes the forecast worse in that region. The contrast in the impact on precipitation between central and eastern Sahel is consistent with the impact on the cold brightness temperatures associated with deep convective clouds in the analysis (see section 3.2).

5 Discussion

The results from the two experiments with and without the enhanced AMMA radiosonde network demonstrate that the impact of the observations on the analysis is significant, in particular in the region of the low-level monsoon flow and the AEJ. However, the effect of the observations on the forecast disappears after only 24 hours. This is believed to be related to the presence of biases in the model. Therefore, the observation impact is limited mainly to the analysis fields. For precipitation, the forecast initialized with analysis containing the AMMA observations is worsened in some regions. AMMA shows an improvement in the precipitation pattern over the central Sahel, but a degradation over the eastern Sahel. In this section, the discussion will focus on three important issues: (i) the presence of biases in the model; (ii) the analysis increments and their role in the degradation of the forecast; and (iii) the lack of observations in the eastern part of Sahel.

5.1 The Model bias

The mean analysis increments presented in the previous section indicate that there is a very large temperature bias at low-levels over the Sahel. The variability of the temperature analysis increments reflects the diurnal cycle of the model temperature bias. Boundary layer temperature is modulated by the net radiation, the Bowen ratio and the advection by the monsoon flow. Guichard (2008) presented evidence of a large bias in the net radiation at a site in the Sahel (Agougou at 11^{o}W and 15^{o}N) which could easily explain the bias in temperature (see Guichard *et al.* (2009) for more details on the site measurements). Possible reasons for this net radiation bias were pointed out by Guichard *et al.* (2009) including model deficiencies in cloud cover, precipitation and aerosol, as well as the need to improve the surface scheme, in particular the representation of vegetation. It is well known that the ECMWF model has problems in the cloud and precipitation over West Africa with the ITCZ being shifted to the south and an overall lack of precipitation over Sahel (Agustí-Panareda and Beljaars, 2008; Agustí-Panareda *et al.*, 2009b). This negatively feeds back on the soil moisture which has a large deficit over the Sahel (Agustí-Panareda *et al.*, 2009a; de Rosnay *et al.*, 2005) and also on the incoming solar radiation as shown by Guichard (2008). It is likely that this radiation bias is having a first order effect on boundary layer temperature. The feedback between excess of net radiation, temperature warm bias and dry bias at low- and mid-levels is enhancing the cloud bias by hindering the formation of cloud. This would loop back into the radiation bias, preventing any possibility of precipitation over the Sahel. The Saharan dust aerosols have also been proven to play an important role on the west African monsoon. Tompkins *et al.* (2005) and Rodwell and Jung (2008) presented large impacts on the AEJ and the precipitation over West Africa from changes in the aerosol climatology. In the future, the coupling of aeorosol forecast with radiation is expected to improve the bias in the net radiation and precipitation through the physical and dynamical feedbacks in the Saharan heat low system during the wet monsoon season.

5.2 Analysis increments and their impact on the forecast

The temperature bias in the model (see section 5.1) results in large low-level temperature analysis increments, which in turn produce divergent wind increments and sinking motion below 700 hPa. As a first step to assess the cause of these divergent wind increments, the AMMA analysis experiment was performed with univariate divergence in the background error covariance matrix or B-matrix (see section 2). This means that temperature increments cannot result in divergent wind increments through the balance specified in the B-matrix. The results from this experiment showed no significant change in the divergent wind increments. This is in accordance with the changes made by Derber and Bouttier (1999) which effectively reduced the balance in the B-matrix for the tropics. Thus, the divergent and subsiding analysis increments around several stations in the data-sparce areas of the Sahel (e.g. N'Djamena, Agadez and Tomboctou) are caused by the model and not the assimilation system. It appears that the reduction in temperature is producing cool temperature anomalies around the radiosonde stations which result in thermally driven circulations. These subsiding and diverging circulations constitute a deterrent for the triggering of convection, also explaining why the precipitation forecasts did not improve over the data-sparse regions.

5.3 The African easterly jet over the data-scarse eastern Sahel

It is clear that the wind observations at 700 hPa are contributing to the change of the AEJ structure in the ECMWF analysis, particularly at the jet entrance and northern flank of the AEJ. AMVs show that the jet streak indeed appears to extend all the way to the Red Sea. Thus, the winds in the eastern part of the tropical north Africa are likely to be too weak in the model analyses. This could have important consequences for prediction of African easterly wave (AEW) activity in the region on daily-to-medium range timescales. First, since some

AEWs clearly develop in this eastern region, it is possible that the current observing system fails to pick up AEWs in their early stages of development. Analysing them sooner will likely have significant benefits for downstream prediction. Also, recent analyses of AEWs suggests that they are triggered by finite amplitude diabatic forcing (Berry and Thorncroft, 2005) that is most commonly linked to topography (see Mekonnen *et al.*, 2006). Thorncroft *et al.* (2008) showed using an idealized dry adiabatic model, that imposed transient diabatic heating can trigger an AEW downstream as well as increase the overall AEW-activity for several days after. This is due to a projection of the perturbation on the most unstable mode for the zonally varying basic state (Hall *et al.*, 2006). The amplitude of the downstream AEW response depends on the location of the heating with respect to the AEJ (Thorncroft *et al.*, 2008) and the nature of the AEJ itself (Leroux and Hall, 2009). Hence, these observational and modeling studies motivate the need to represent the AEJ in NWP models as accurately as possible. If the AEJ was strengthened in the east, this would likely mean that AEWs could develop sooner, in association with convection in the Ethiopian highlands for example.

6 Conclusions and future work

Radiosondes are the only observing system that provide a full description of atmospheric profile in the lower and mid-troposphere in the ECMWF analysis. It is therefore not surprising that the AMMA radiosonde observations have a significant impact on the ECMWF analysis. On the other hand, the influence on the forecast is very short-lived due to large model biases. The AMMA radiosonde observations are crucial to detect these model biases. Mean analysis increments indicate that there is a very large model bias in low-level temperature over Sahel consistent with a bias in net radiation, lack of cloud cover and precipitation. These model biases make the 4DVar data assimilation non-optimal, as the 4DVar scheme used here assumes a perfect model in the 12-hours assimilation window.

The mean analysis differences between AMMA and pre-AMMA experiments show a large impact of the radiosonde observations on the low-level temperature over Sahel and the AEJ. The impact is particularly pronounced in northern and eastern Sahel. Comparison with AMVs leads to the conclusion that over eastern Sahel the AEJ is too weak in the ECMWF model. There are important implications of having a weaker AEJ in the model forecast for the development of African easterly waves. As future work, experiments could be performed to test the impact of assimilating AMVs in the region of the AEJ, in particular over eastern Sahel where there are no other observations available.

There is an overall improvement in the cloud and precipitation in the AMMA experiment with an increase of deep cloud in the analysis and a precipitation increase in the 1-day forecast between 10^o W and 10 ^{o} E. However, there is a decrease of both cloud and precipitation east of 15^oE over Sahel where there is deficit in the model. Thus, although the mean analysis/forecast is improved over central Sahel, it is actually degraded over eastern Sahel. The degradation is caused by unrealistic analysis increments of winds that are the result of large temperature increments. These wind increments are divergent and result in enhanced subsidence in the analysis which has an unfavourable feedback on the cloud and temperature bias. They can also explain the negative impact of the extra observations in the data-sparce region north of 15^oN and east of 15^oE. In order to make good use of the observations further work needs to be done to reduce the bias in cloud and surface temperature over the region of Sahel (e.g. by including aerosol coupling with radiation).

Acknowledgements

Based on a French initiative, AMMA was built by an international scientific group and is currently funded by a large number of agencies, especially from France, UK, US and Africa. It has been beneficiary of a major financial contribution from the European Community's Sixth Framework Programme. Detailed information on scientific coordination and funding is available on the AMMA international web site "http://www.amma-international.org".

The authors would like to thank Milan Dragovac for his help in converting all the AMMA sounding data to BUFR format; Drasko Vasiljevic and Jan Haseler for their technical advice and support on the data assimilation experiments; Paul Poli for his suggestion on the use of AMVs; Lars Isaksen for his support on OBSTAT and feedback on the use of AMVs; Mike Fisher for his advice on the diagnostics and interpretation of the analysis increments, as well as providing his branch for the J_b modification experiment; Doug Parker for kindly providing Fig. 1; Jan Polcher for his feedback on the manuscript; Alan Geer for his advice and help on the computation of the scores; the ECMWF metview team for their graphics support and Martin Köhler, Maike Ahlgrimm, Philippe Lopez, Richard Forbes and Peter Bechtold for their fruitful discussions on the material presented in this paper.

References

Agustí-Panareda A, Balsamo G, Beljaars A. 2009a. Impact of improved soil moisture on the ECMWF precipitation forecast in West Africa. *Geophys. Res. Lett* (submitted).

Agustí-Panareda A, Beljaars A. 2008. ECMWF's contribution to AMMA. *ECMWF Newsletter* **No. 115**: 19–27.

Agustí-Panareda A, Vasiljevic D, Beljaars A, Bock O, Guichard F, Nuret M, Lafore JP, Mendez AG, Andersson E, Bechtold P, Fink A, Hersbach H, Ngamini JB, Parker D, Redelsperger JL, Tompkins A. 2009b. Radiosonde humidity bias correction over the West African region for the special AMMA reanalysis at ECMWF. *Quart. J. Roy. Meteor. Soc.* **135**: 595–617.

Bechtold P, Köhler M, Jung T, Leutbecher M, Rodwell M, Vitart F. 2008. Advances in simulating atmospheric variability with ifs cycle 32r3. *ECMWF Newsletter* **No. 114**: 29–38.

Berry G, Thorncroft C. 2005. Case study of an intense African easterly wave. *Mon. Wea. Rev.* **133**: 752–766.

de Rosnay P, Boone A, Beljaars A, Polcher J. 2005. AMMA Land-Surface modeling and Intercomparison Projects. *GEWEX News* **16**: 10–11.

Derber J, Bouttier F. 1999. A reformulation of the background error covariance in the ECMWF global data assimilation system. *Tellus-A* **51**: 195–221.

Faccani C, Rabier F, Fourrie N, Agustí-Panareda A, Karbou F, Moll P, Lafore JP, Nuret M, Hdidou F, Bock O. 2009. The impact of the AMMA radiosonde data on the french global assimilation and forecast system. *Wea. Forecasting* Doi:10.1175/2009WAF2222237.1 (In press).

Gauthier P, Thépaut JN. 2001. Impact of the digital filter as a weak constraint in the pre-operational 4dvar assimilation system at météo-france. *Mon. Wea. Rev.* **129**: 2089–2102.

Guichard F. 2008. What can we learn from AMMA about physical processes and models? Seminar on parametrization of subgrid physical processes, 1-4 september, ECMWF, Shinfield Road, Reading, UK.

Guichard F, Kergoat L, Mougin E, Timouk F, Baup F, Hiernaux P, lavenu F. 2009. Surface thermodynamics and radiative budget in the sahelian gourma: seasonal and diurnal cycles. *J. Hydrology* (in press) doi:10.1016/j.jhydrol.2008.09.007.

Hall N, Kiladis G, Thorncroft C. 2006. Three dimensional strucutre and dynamics of African easterly waves. part ii: Dynamical modes and growth mechanisms. *J. Atmos. Sci.* **63**: 2231–2245.

Janisková M, Mahfouf JF, Morcrette JJ, Chevallier F. 2002. Linearized radiation and cloud schemes in the ECMWF model: Development and evaluation. *Quart. J. Roy. Meteor. Soc.* **128**: 1505–1527.

Janisková M, Thépaut JN, Geleyn J. 1999. Simplified and regular physical parametrizations for incremental four-dimensional variational assimilation. *Mon. Wea. Rev.* **127**: 26–45.

Leroux S, Hall N. 2009. On the relationship between african easterly waves and the african easterly jet. *J. Atmos. Sci.* (in press).

Lopez P, Moreau E. 2005. A convection scheme for data assimilation: Description and initial tests. *Quart. J. Roy. Meteor. Soc.* **131**: 409–436.

Mari C, Cailley G, Corre L, Saunois M, Attié J, Thouret V, Stohl A. 2008. Tracing biomass burning plumes from the southern hemisphere during the AMMA 2006 wet season experiment. *Atmos. Chem. Phys.* **8**: 3951–3961.

Mekonnen A, Thorncroft C, Aiyyer A. 2006. On the significance of African easterly waves on convection. *J. Climate* **19**: 5405–5421.

Parker DJ, Fink A, Janicot S, Ngamini JB, Douglas M, Afiesimama E, Agustí-Panareda A, Beljaars A, Dide F, Diedhiou A, Lebel T, Polcher J, Redelsperger JL, Thorncroft C, Wilson GA. 2008. The AMMA radiosonde programme and its implications for the future of atmospheric monitoring over Africa. *Bull. Amer. Metero. Soc.* **89**: 1015–1027.

Rabier F, Järvinen H, Klinker E, Mahfouf JF, Simmons A. 2000. The ECMWF operational implementation of four-dimensional variational assimilation. i: Experimental results with simplified physics. *Quart. J. Roy. Meteor. Soc.* **126**: 1143–1170.

Rodwell M, Jung T. 2008. Understanding the local and global impacts of model physics changes. Seminar on parametrization of subgrid physical processes, 1-4 september, ECMWF, Shinfield Road, Reading, UK.

Thorncroft C, Hall N, Kiladis G. 2008. Three-dimensional structure and dynamics of African easterly waves. part iii: Genesis. *J. Atmos. Sci.* **65**: 3596–3607.

Thorncroft C, Parker D, Burton R, Diop M, Ayers J, Bariat H, Devereau S, Diongue A, Dumelow R, Kindred D, Price N, Saloum M, Taylor C, Tompkins A. 2003. The jet2000 project: Aircraft observations of the african easterly jet and the African easterly waves. *Bull. Amer. Metero. Soc.* **84**: 337–351.

Tompkins A, Cardinali C, Morcrette JJ, Rodwell M. 2005. Influence of aerosol climatology on forecasts of the African Easterly Jet. *Geophysical Research Letters* **32**: 1–4. Doi:10.1029/2004GL022189.

Tompkins A, Janisková M. 2004. A cloud scheme for data assimilation: Description and initial tests. *Quart. J. Roy. Meteor. Soc.* **130**: 2495–2518.

Velden C, Bedka K. 2009. Identifying the uncertainty in determining satellite-derived atmospheric motion vector height attribution. *J. Appl. Met. Clim.* **21**: 921–932.

Velden C, Daniels J, Stettner D, Santek D, Key J, Dunion J, Holmlund K, Dengel G, Bresky W, Menzel P. 2005. Recent innovations in deriving tropospheric winds from meteorological satellites. *Bull. Amer. Metero. Soc.* **86**: 205–223.

von Bremen L. 2005. Characterization and use of atmospheric motion vectors at ECMWF. Technical report, EUMETSAT/ECMWF Fellowship Programme Report.

Wang J, Cole HL, Carlson DJ, Miller ER, Beierle K. 2002. Corrections of humidity measurement error from the vaisala rs80 radiosonde - application to toga coare data. *J. Atmos. Oceanic Technol.* **19**: 981–1002.

Table 1: Enhanced AMMA radiosonde network during August 2006. The number of daily soundings planned in parenthesis refers to the intensive observing period between 1st and 15th of August 2006.

Station name	WMO station ID	Lat [^{o}N]	Lon [^{o}E]	Altitude [m]	Number of soundings planned per day	Total number of soundings	High resolution data
Sal	08594	16.73	-22.95	53	1	31	No
Tamanrasset	60680	22.80	5.43	1364	4	123	No
Agadez	61024	16.97	7.98	502	4 (8)	183	Yes
Niamey	61052	13.48	2.17	227	4 (8)	179	Yes
Tombouctou	61223	16.72	-3.00	264	2	44	Yes
Bamako/Senou	61291	12.53	-7.95	381	2	62	Yes
Nouadhibou	61415	20.93	-17.03	3	1	1	Yes
Nouakchott	61442	18.10	-15.95	3	1	24	Yes
Dakar/Yoff	61641	14.73	-17.50	24	2	58	Yes
Tambacounda	61687	13.77	-13.68	50	1	44	Yes
Conakry	61831	9.56	-13.61	48	1	1	Yes
Addis Ababa-Bole	63450	9.03	38.75	2354	1	23	No
Bangui	64650	4.40	18.52	366	2	8	Yes
N'Djamena	64700	12.13	15.03	295	2	46	Yes
Ngaoundere	64870	7.35	13.57	1104	1	33	Yes
Douala R.S	64910	4.02	9.70	15	2	27	Yes
Abuja	65125	9.25	7.00	344	4 (8)	158	Yes
Parakou	65330	9.35	2.62	393	4 (8)	171	Yes
Cotonou	65344	6.35	2.38	9	4 (8)	178	Yes
Tamale	65418	9.50	-0.85	173	4 (8)	174	Yes
Ouagadougou	65503	12.35	-1.52	306	2	63	Yes
Abidjan	65578	5.25	-3.93	8	2	79	Yes

Table 2: Pre-AMMA radiosonde network

Station name	WMO station ID	Lat [^{o}N]	Lon [^{o}E]	Altitude [m]	Number of soundings planned per day	Total number of soundings	High resolution data
Sal	08594	16.73	-22.95	53	1	26	No
Tamanrasset	60680	22.80	5.43	1364	2	61	No
Agadez	61024	16.97	7.98	502	1	19	No
Niamey	61052	13.48	2.17	227	2	46	No
Bamako/Senou	61291	12.53	-7.95	381	2	50	No
Dakar/Yoff	61641	14.73	-17.50	24	2	49	No
Douala R.S	64910	4.02	9.70	15	2	4	No
Ouagadougou	65503	12.35	-1.52	306	1	23	No

Table 3: Atmospheric motion vector U-component bulk statistics against radiosondes in the vicinity (+/- 1^o) of two radiosonde stations in the region of the African easterly jet core. Vertical levels used span between 750 and 500 hPa.

Station name	Lat [^{o}N]	Lon [^{o}E]	Mean AMV	Mean RS	Std. dev. AMV	Std. dev. RS	Median RS	Median AMV	N RS	N
N'Djamena	12.13	15.03	-10.3	-11.0	3.4	5.0	-11.5	-9.6	140	550
Niamey	13.48	2.17	-11.0	-11.8	4.6	4.8	-10.2	-12.1	285	4413
Tombouctou	16.72	-3.00	-13.0	-11.8	4.8	5.0	-13.3	-12.0	97	1063
Ouagadougou	12.35	-1.52	-10.2	-10.8	5.0	5.7	-10.6	-11.0	107	1602

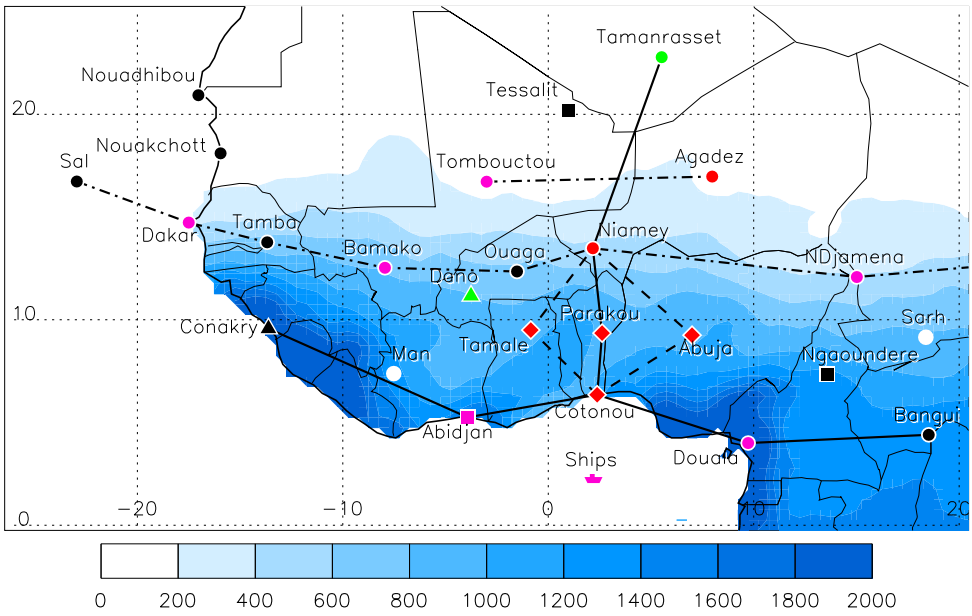

Figure 1: Key stations of the AMMA radiosonde network. "Tamba" is Tambacounda and "Ouaga" is Ouagadougou. Shapes denote the status: circles are reactivated stations (or those reconnected to the GTS), and triangles are stations that operated temporarily in 2006 (Praia is not shown, as it is very close to Sal). Color indicates the planned operational frequencies in 2006: white indicates operational (1 per day) with no GTS communicaitons, black indicates 1 per day, magenta 2 per day, green 4 per day (Tamanrasset) or variable (Dano) and red achieved 4 per day during SOPs 1-3, with 8 per day during IOPs. Refer to Table 2 for more details. The observed mean annual precipitation amount for the period 1961-90 is contoured (up to 2,000 mm yr^{-1}, based on the VASClimo dataset (Beck et al. 2005). The "monsoon" transets are denoted by solid lines, the "zonal" and northern transects are dash-dotted, and the "southern quadrilateral" is dashed. From Parker et al. (2008).

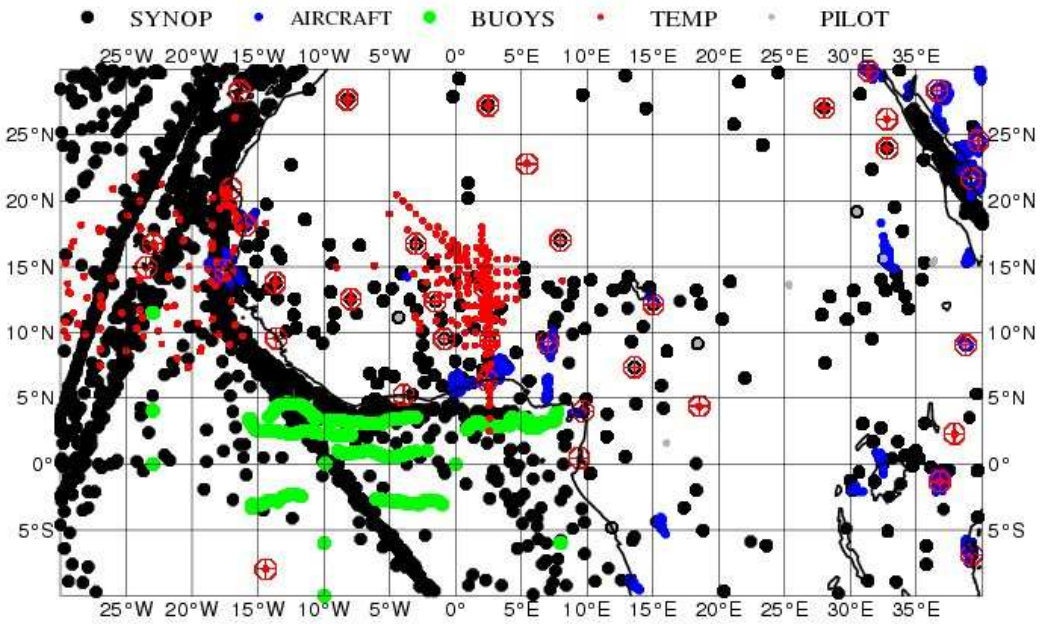

Figure 2: Map showing spatial coverage of conventional observation types (SYNOP from land and ship meteorological stations, aircrafts, buoys, TEMP from radiosondes and dropsondes, and PILOT balloons) used in the ECMWF analysis experiments below 500 hPa during August 2006. Radiosondes are highlighted with a large cross and circle; small red dots are dropsondes. Only the number TEMP messages available varies between the two experiments presented in this paper, particularly the radiosondes.

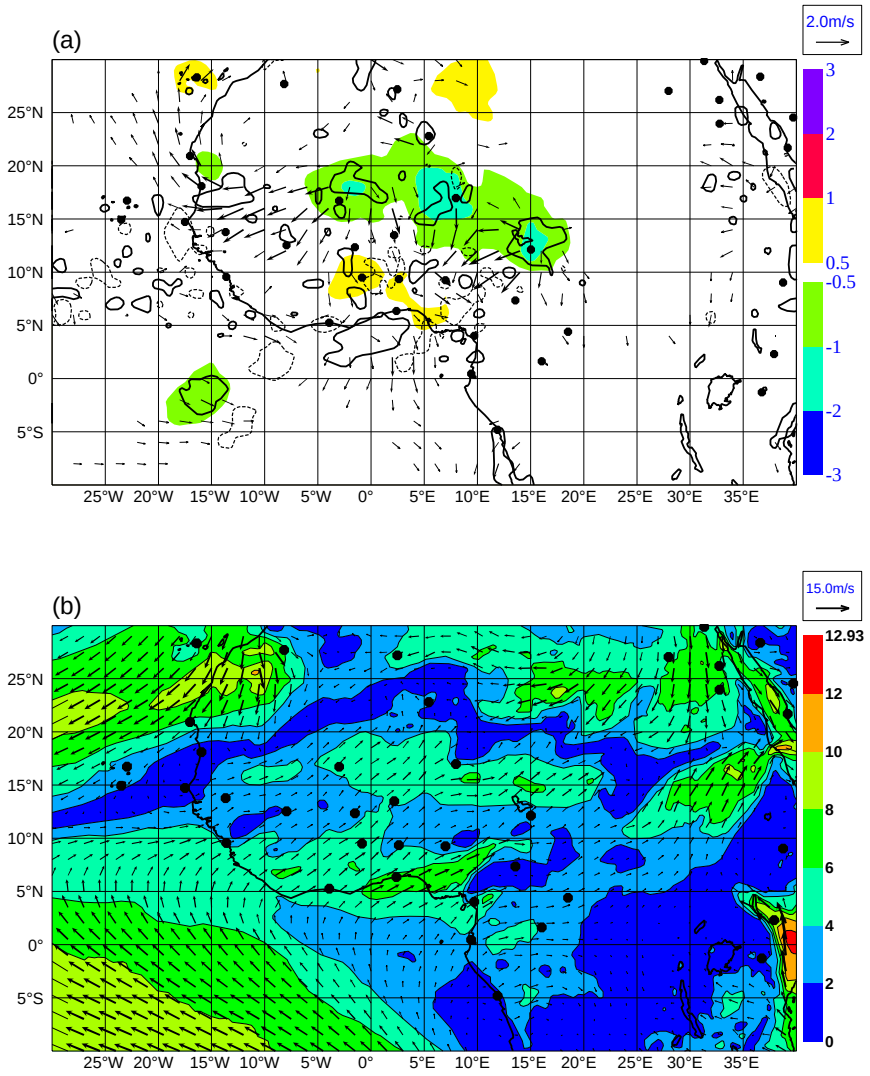

Figure 3: (a) Mean temperature analysis increments at 925 hPa for August 2006 based on both the 00 UTC 12 UTC analysis from the AMMA experiment; the arrows depict the wind analysis increments and the black lines are the vertical velocity contours of 0.025 Pa/s (solid line) and -0.025 Pa/s (dash line) at the same level and time. (b) Mean wind vector analysis (see arrow legend) and mean wind speed (see colour scale) at 925 hPa from 00 UTC and 12 UTC for August 2006 (AMMA experiment). The black dots depict the location of the AMMA radiosonde stations.

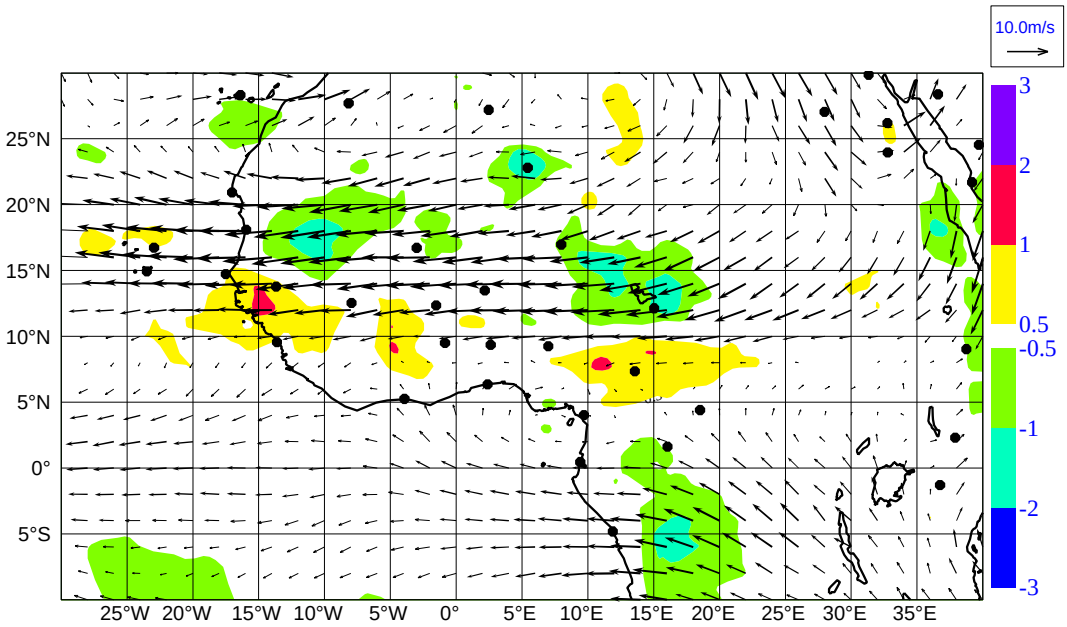

Figure 4: Mean zonal wind analysis increments at 700 hPa for August 2006 based on both the 00 UTC and 12 UTC analyses from the AMMA experiment (in shading). The arrows depict the mean wind vector analysis at the same level and time.The black dots depict the location of the AMMA radiosonde stations.

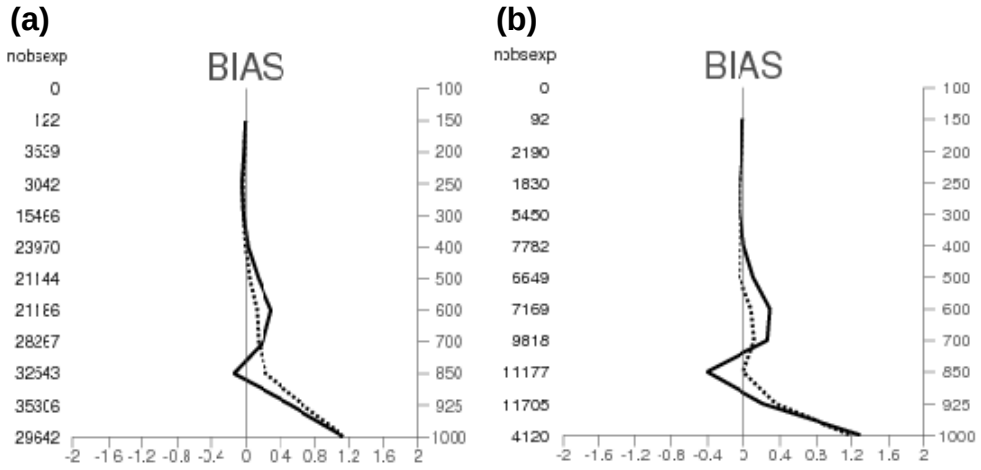

Figure 5: Mean vertical profile of radiosonde observation-background departures (OB-BG, solid line) and radiosonde observation-analysis departures (OB-AN, dashed line) of specific humidity [g Kg^{-1}] for the AMMA analysis over (a) the whole West African region (5°N–30°N, 20°W–20°E) and (b) the Sahel region (12°N–22°N, 20°W–20°E). Numbers indicate the number of observations available.

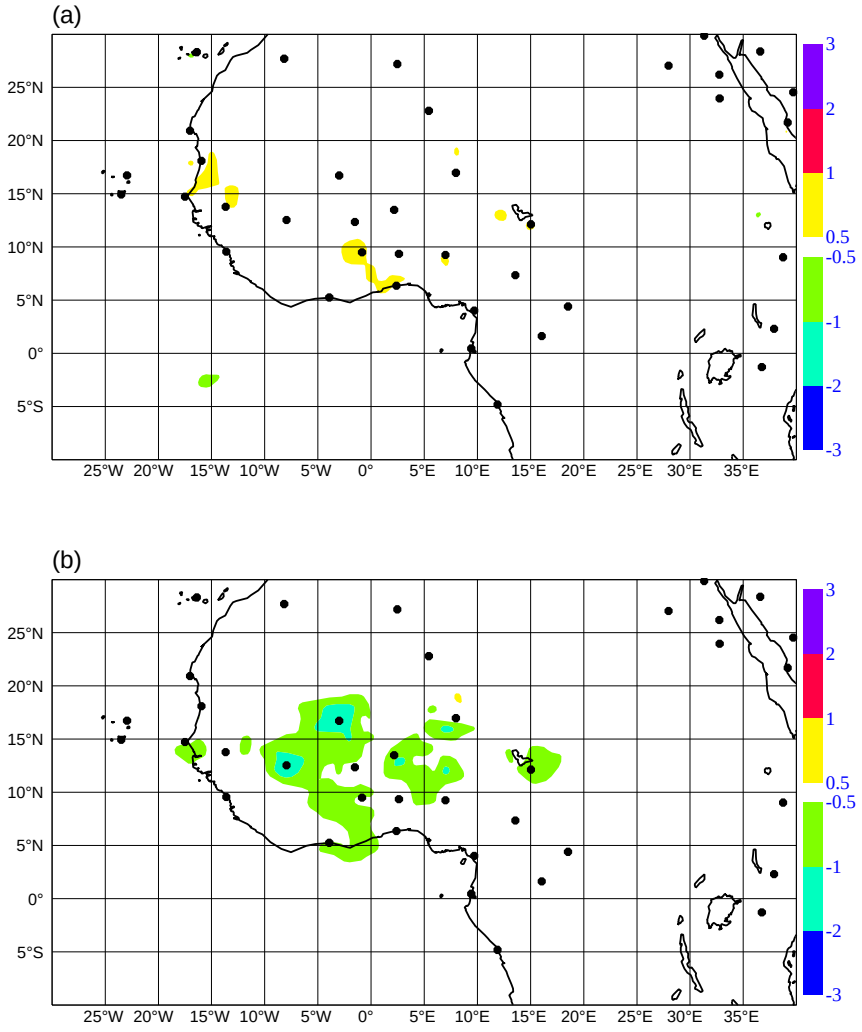

Figure 6: Mean specific humidity analysis increments [g Kg^{-1}] at (a) model level 84 (near 925 hPa) and (b) model level 79 (near 850 hPa) for August 2006 based on both the 00 UTC and 12 UTC analyses from the AMMA experiment. The black dots depict the location of the AMMA radiosonde stations.

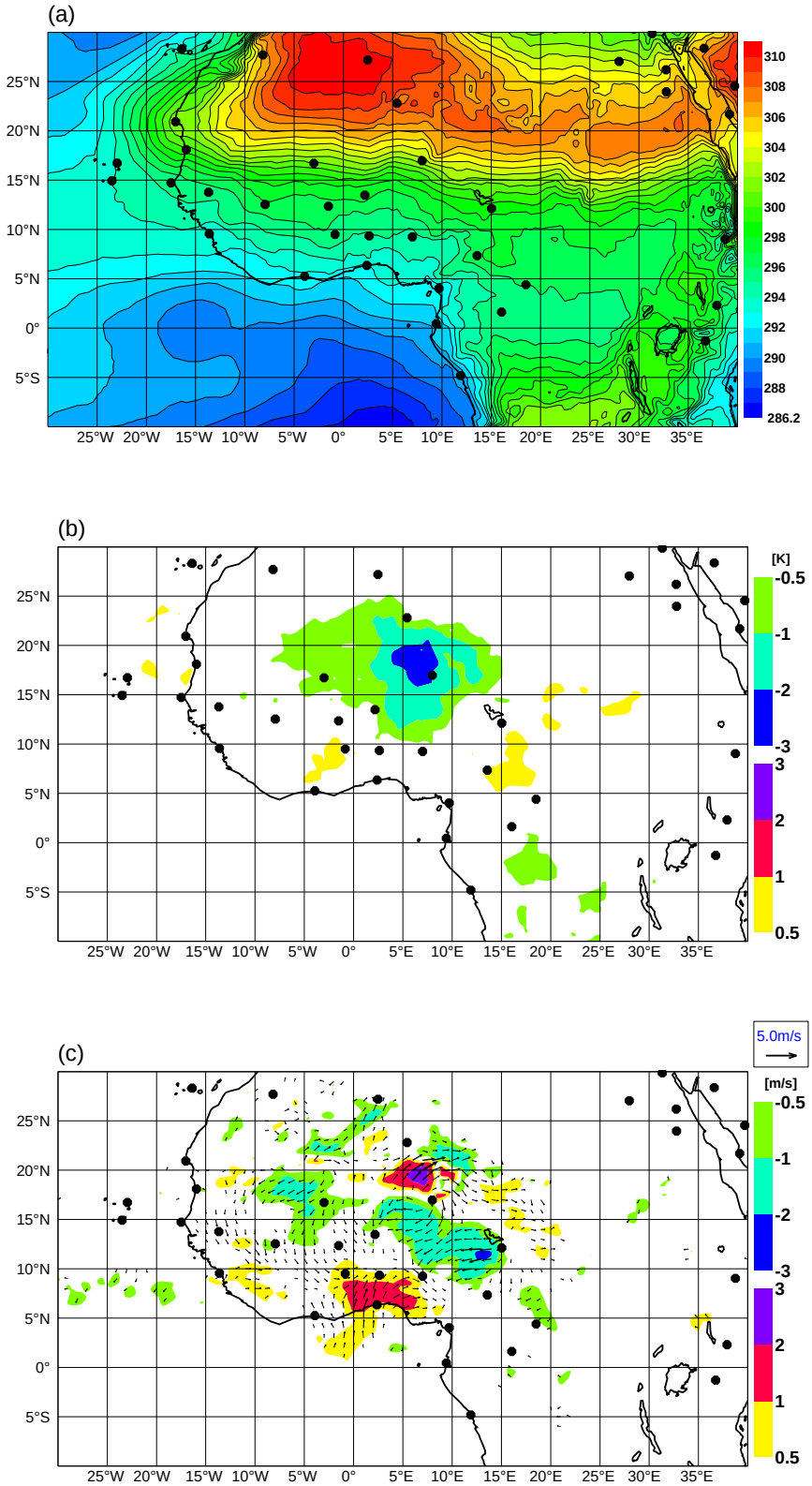

Figure 7: (a) Mean temperature [K] at 925 hPa for August 2006 based on 00 and 12 UTC analyses from the AMMA experiment. The difference between the AMMA and pre-AMMA experiments for (b) mean temperature at 925 hPa [K] and (c) mean wind from 00 and 12 UTC analyses. The colour shading in (c) indicates the difference in mean wind speed and the arrows depict the mean difference in wind vectors. The black dots show the location of the AMMA radiosonde stations.

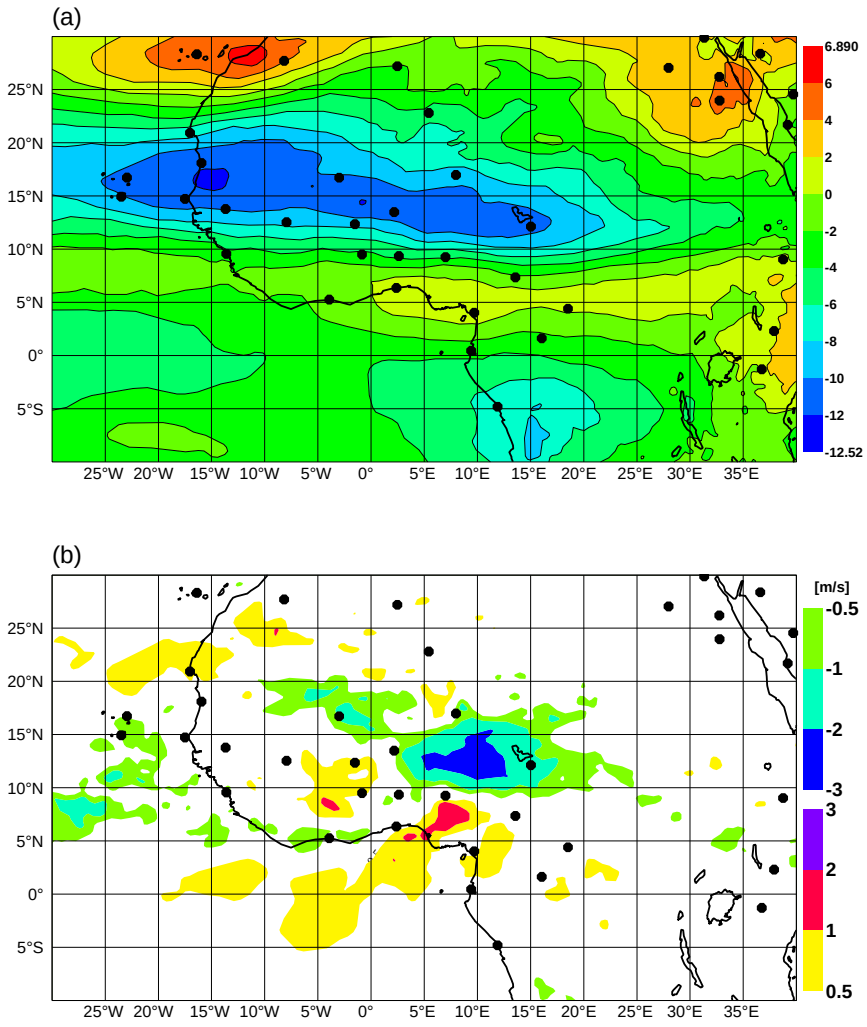

Figure 8: (a) Mean analysis for the AMMA experiment and (b) difference between the two experiments (AMMA minus pre-AMMA) for the zonal wind at 700 hPa from 00 UTC and 12 UTC analyses for August 2006. The black dots indicate the location of the AMMA radiosonde stations.

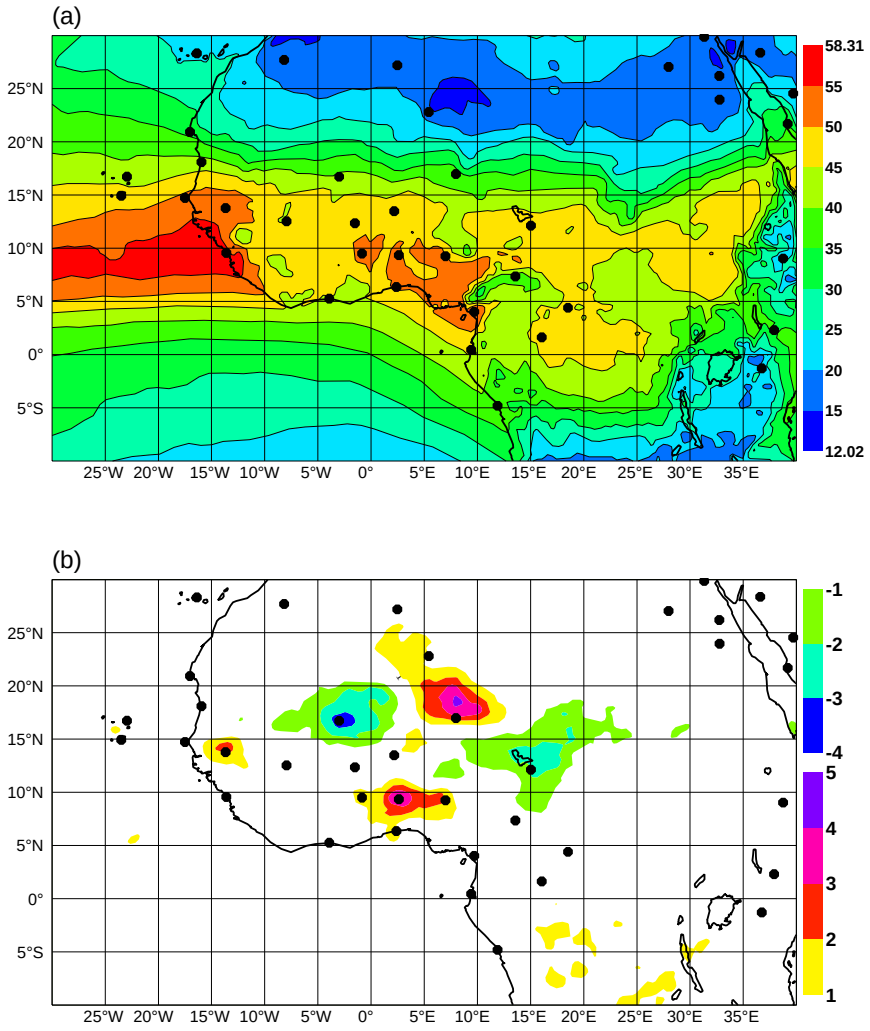

Figure 9: (a) Mean analysis for the AMMA experiment and (b) difference between the two experiments (AMMA minus pre-AMMA) for total column water vapour [kg m^{-2}] from 00 and 12 UTC analyses for August 2006. The black dots indicate the location of the AMMA radiosonde stations.

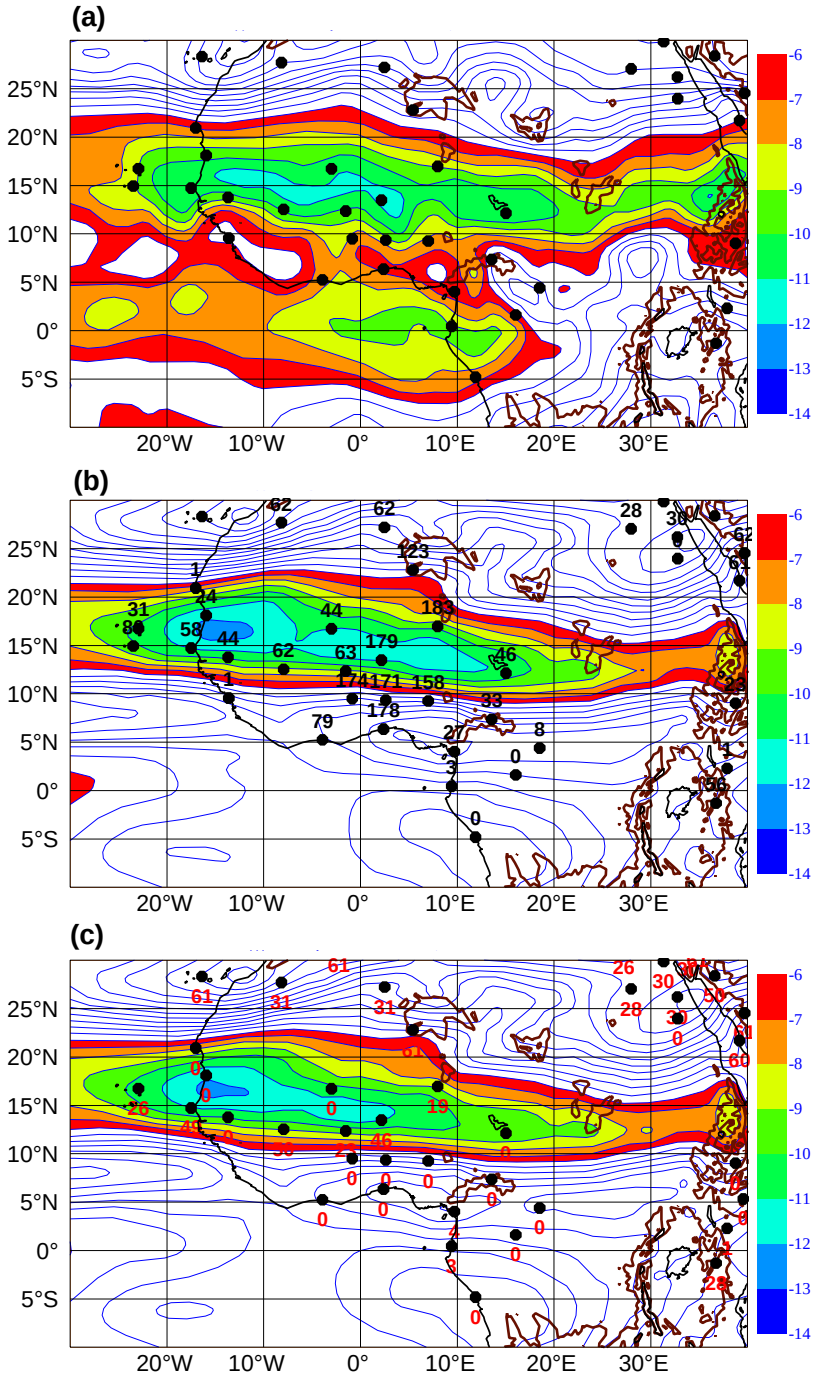

Figure 10: Mean zonal wind (1 m s^{-1} contour inverval) within the layer between 750 and 500 hPa for August 2006 from: (a) atmospheric motion vectors from Meteosat-8 gridded with $2^o \times 2^o$ resolution, (b) the AMMA and (c) the pre-AMMA analyses. The analysis data has also been plotted in a grid with 2×2 degrees resolution for comparison purposes. The black dots indicate the location of the AMMA radiosonde stations and the numbers depict the number of soundings used.

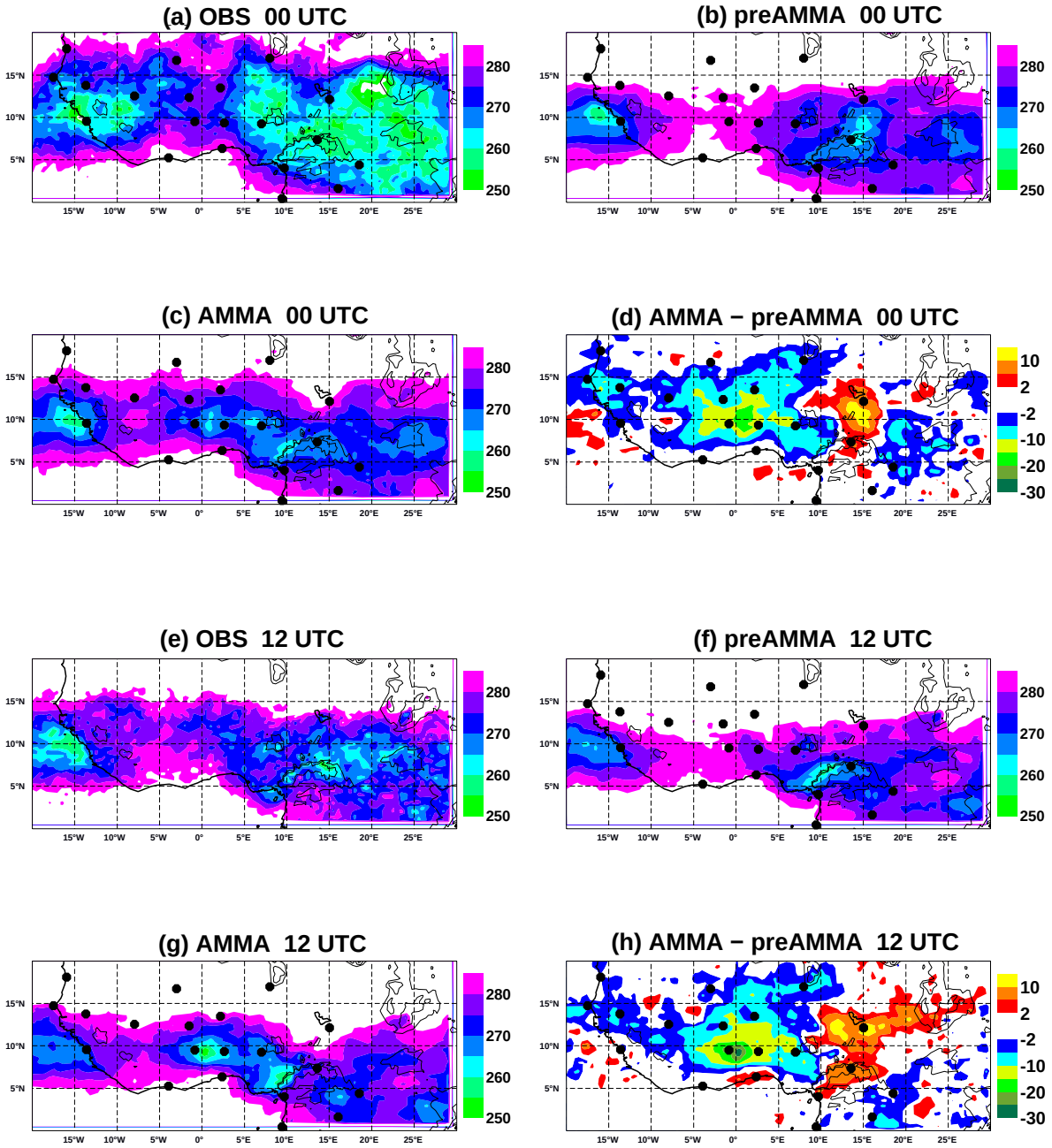

Figure 11: Mean brightness temperatures [K] (channel 10.8 µm) for August 2006 at 00 UTC and 12 UTC from: (a,e) observations (Meteosat); (b,f) pre-AMMA analysis; (c,g) AMMA analysis; and (d,h) the difference between the analysis experiments (AMMA - pre-AMMA). The contour lines on (a,b,c,e,f,g) represent orography with contours at 700 m, 1000 m, 2000 m and every 500 m thereafter. The black dots depict the location of the AMMA radiosonde stations.

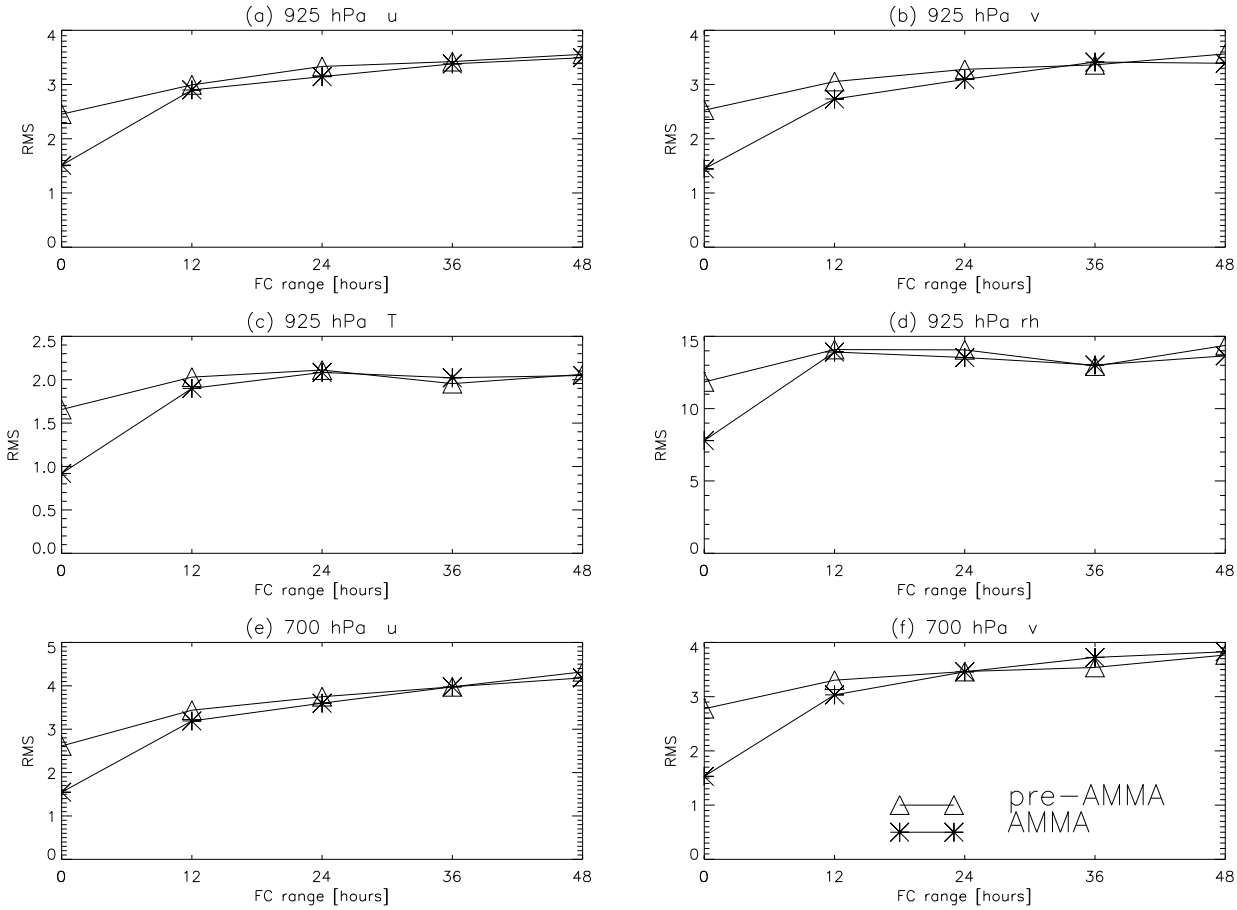

Figure 12: Root mean square error of forecast from the AMMA (asterisks) and pre-AMMA (triangles) experiments with respect to radiosonde observations for different parameters within a region between 10°N and 20°N and 20°W to 20°E: (a) zonal wind [m s^{-1}] at 925 hPa; (b) meridional wind [m s^{-1}] at 925hPa; (c) temperature [K] at 925 hPa; (d) relative humidity [%] at 925 hPa; (e) zonal wind [m s^{-1}] at 700 hPa; (f) meridional wind [m s^{-1}] at 700 hPa.

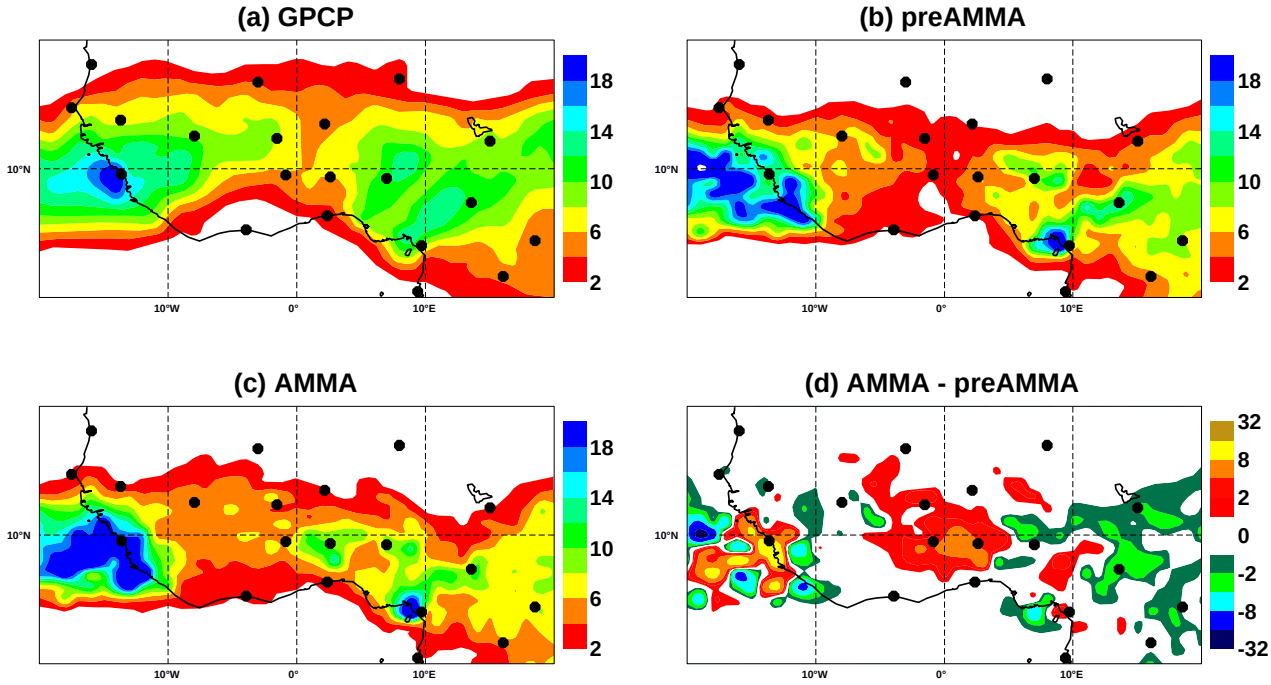

Figure 13: Mean precipitation 1-day precipitation [mm day^{-1}] forecast (T+36 - T+12) for the period 3rd August to 2nd September 2006 from (a) the Global Precipitation Climate Project dataset (GPCP) from NCEP/NOAA derived from satellite observations; (b) pre-AMMA; (c) AMMA; and (d) the difference between the two experiments (AMMA - pre-AMMA). The black dots indicate the location of the AMMA radiosonde stations.